

A Photometric Study of the Eclipsing Variable Star NSVS 3068865

Robert C. Berrington

Ball State University, Department of Physics and Astronomy, Muncie, IN 47306; rberrington@bsu.edu

Erin M. Tuhey

Ball State University, Department of Physics and Astronomy, Muncie, IN 47306; emtuhey@bsu.edu

Received May 22, 2014; revised August 13, 2014 and October 26, 2015; accepted November 12, 2015

Abstract We present new multi-band differential aperture photometry of the eclipsing variable star NSVS 3068865. The light curves are analyzed with the Wilson-Devinney model to determine best-fit stellar models. Our models show that NSVS 3068865 is consistent with a W Ursae Majoris eclipsing variable star near thermal contact with similarities to the aforementioned proto-type.

1. Introduction

The star NSVS 3068865 [= TYC 3929-1500-1, R. A. = $19^{\text{h}} 21^{\text{m}} 4.43^{\text{s}}$, Dec. = $+56^{\circ} 19' 41.1''$, J2000.0] was designated [GGM2006] 3068864 by Gettel *et al.* (2006) and found to be an eclipsing variable star by using the photometric data from the Northern Sky Variability Survey (NSVS; Woźniak 2004) with a period of $P = 0.334292$ day. Later, the automated classification system developed by Hoffman *et al.* (2009) classified the star as a W Ursae Majoris contact eclipsing binary and reported a photometric period of $P = 0.33428$ day. The NSVS is a search for variability in the stars observed with the Robotic Optical Transient Search Experiment (ROTSE-1; Woźniak 2004). The primary goal of the NSVS is to search for optical transients associated with quick response to Gamma-Ray Burst (GRB) events reported from satellites to measure optical light curves of GRB counterparts. When no GRB events were available, ROSTE-I was devoted to a systematic sky patrol of the sky northward of declination $\delta = -38^{\circ}$.

In this paper we present a new extensive photometric study of this system. The paper is organized as follows. Observational data acquisition and reduction methods are presented in section 2. Time analysis of the photometric light curve and Wilson-Devinney models are presented in section 3. Discussion of the results and conclusions are presented in section 4.

2. Observational data

We present new three-filter photometry of the eclipsing variable star NSVS 3068865. The data were taken by the Meade 0.4-meter Schmidt Cassegrain telescope within the Ball State University observatory located atop the Cooper science complex. All exposures were acquired by a Santa Barbara Instruments Group (SBIG) STL-6303e camera through the Johnson-Cousins B, V, and R (R_c) filters on the nights of July 12, 13, 14, 16, and 18, 2013. All images were bias and dark current subtracted, and flat field corrected using the CCDRED reduction package found in the Image Reduction and Analysis Facility (IRAF) version 2.16 (IRAF is distributed by the National Optical Astronomy Observatories, <http://iraf.net/>). All photometry presented is differential aperture photometry and was performed on the target eclipsing candidate and two comparison standards by the AIP4WIN (v2.2.0) photometry package (Berry and Burnell

2005). Over the three nights a total of 482 images were taken in B, 486 images in V, and 510 images in R_c . Figure 1 shows a representative exposure with the eclipsing star candidate and the two comparison stars marked. We have chosen the Tycho catalog star (Høg *et al.* 2000) TYC 3929-1375-1 as the primary comparison star (C1). The folded light curves (see section 3.1) for the instrumental differential B, V, and R_c magnitudes are shown in Figure 2, and are defined as the variable star magnitude minus C1 (Variable – C1). Also shown (bottom panel) in Figure 2 is the differential V magnitude of C1 minus the second comparison star (C2, TYC 3929-1366-1), or the check star. The comparison light curve was inspected for variability. None was found.

Measured instrumental B and V differential magnitudes were reduced onto Johnson B and V magnitudes by comparison with known calibrated magnitudes for C1. The star C1 has measured Johnson B and V magnitudes of 11.37 ± 0.07 and 10.66 ± 0.05 , respectively Høg *et al.* (2000). The calibrated

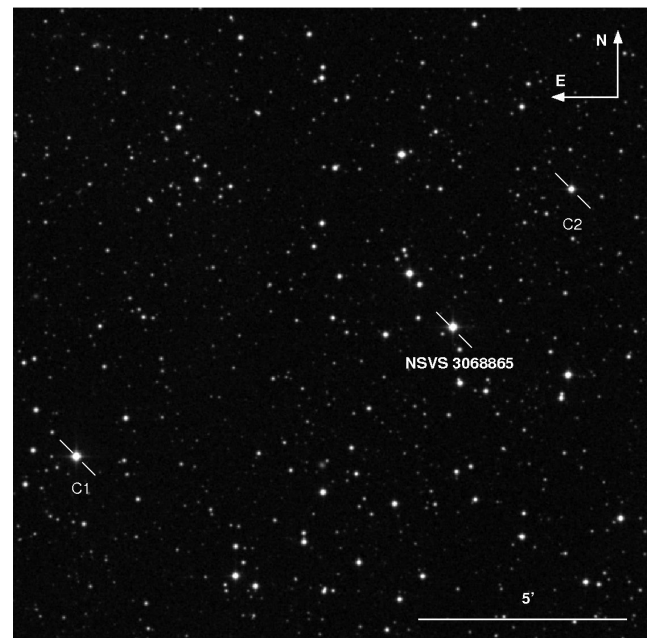


Figure 1. Star field containing the variable star NSVS 3068865. The location of the variable star is shown along with the comparison (C1) star TYC 3929-1375-1 and the check (C2) star TYC 3929-1366-1 used to calculate the differential magnitudes reported in Figure 2.

V light curve with the (B–V) color index versus orbital phase is shown in Figure 3 with error bars removed for clarity. The orbital phase (Φ) is defined as:

$$\Phi = \frac{T - T_0}{P} - \text{Int} \left(\frac{T - T_0}{P} \right), \quad (1)$$

where T_0 is the ephemeris epoch and is the time of minimum of a primary eclipse. Throughout this paper we will use the value of 2456487.66872 for T_0 . The variable T is the time of observation, and P is the period of the orbit. The value of Φ ranges from a minimum of 0 to a maximum of 1.0. All light curve figures will plot phase values (–0.6, 0.6) where the negative values are given by $\Phi - 1$. Simultaneous B and V magnitudes are used to determine (B–V) colors by linear interpolating between measured B magnitudes to a similar time for measured V magnitudes.

3. Analysis

3.1. Period analysis and ephemerides

Heliocentric Julian dates (HJD) for the observed times of minimum were calculated for each of the B, V, and R_c band light curves shown in Figure 2 for all observed primary and secondary minima. A total of three primary eclipses and three secondary eclipses were observed for each band. The times of minimum are determined by the algorithm described by Kwee and van Woerden (1956). Similar times of minimum from differing band passes were compared and no significant offsets or wavelength-dependent trends were observed. Similar times of minimum from each of the band passes were averaged together and reported in Table 1 along with 1σ error bars.

Light curves were inspected by the PERANSO (v2.5) software (CBA Belgium Observatory 2011) to determine the orbital period by applying the analysis of variance (ANOVA) statistic, which uses periodic orthogonal polynomials to fit observed light curves (Schwarzenberg-Czerny 1996). Our best-fit orbital period was found to be 0.33440 ± 0.00037 day and is consistent ($<1\sigma$) with the orbital period reported by Hoffman *et al.* (2009), which uses the photometric data reported by the NSV survey (Woźniak 2004). The resulting linear ephemeris becomes

$$T_{\min} = 2456487.66872(26) + 0.33440(37)E \quad (2)$$

where the variable E represents the epoch number, and is a count of orbital periods from the epoch $T_0 = 2456487.66872$. Figure 2 shows the folded differential magnitudes versus orbital phase for NSVS 3068865 for the B, V, and R_c Johnson-Cousins bands folded over the period determined by the current photometric study.

The observed minus calculated residual times of minimum (O–C) were determined from Equation 2 and are given in Table 1 along with 1σ error bars. The best-fit linear line determined by a linear regression to the (O–C) residual values is shown in Figure 11, and indicates the times of minima are well described by an orbital period of 0.33438 ± 0.00040 day, and is consistent with our previously determined value from

Table 1. Calculated heliocentric Julian dates (HJD) for the observed times of minimum for NSVS 3068865.

T_{\min}	Eclipse	E	(O–C)
2456487.66872 \pm 0.00026	p	0	0
2456487.83712 \pm 0.00019	s	0.5	0.00112 \pm 0.00030
2456489.67456 \pm 0.00019	p	6	0.00056 \pm 0.00029
2456489.84345 \pm 0.00017	s	6.5	0.00113 \pm 0.00029
2456491.68105 \pm 0.00014	p	12	-0.00047 \pm 0.00046
2456491.84843 \pm 0.00033	s	12.5	-0.00029 \pm 0.00056

Notes: Calculated heliocentric Julian dates (HJD) for the observed times of minimum (column 1) with the type of minima (column 2). Observed minus Calculated (O–C) residual (column 4) values are given for the linear ephemeris given in Equation 2. All reported times are averaged from the individual B-, V-, and R-band times of minimum determined by the algorithm described by Kwee and van Woerden (1956). All (O–C) values are given in units of days with primary eclipse values determined from integral epoch numbers, and secondary eclipse values determined from half integral epoch numbers (column 3).

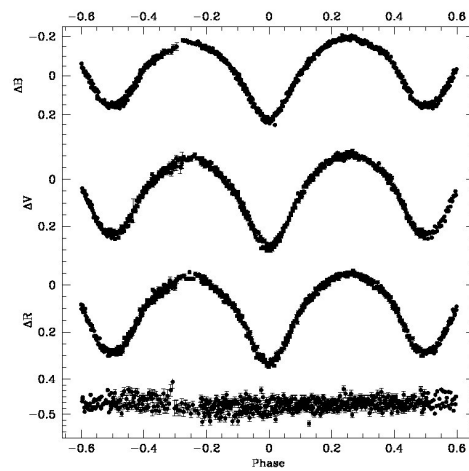


Figure 2. Folded light curves for differential aperture Johnson-Cousins B-, V-, and R_c -band magnitudes. Phase values are defined by Equation 1. Top three panels show the folded light curves for Johnson B (top panel), Johnson V (middle panel), and Cousins R_c (bottom panel) magnitudes. Bottom panel shows differential Johnson V-band magnitudes for the comparison minus the check star. All error bars are 1σ error bars. Repeated points do not show error bars (points outside the phase range of (–0.5, 0.5)).

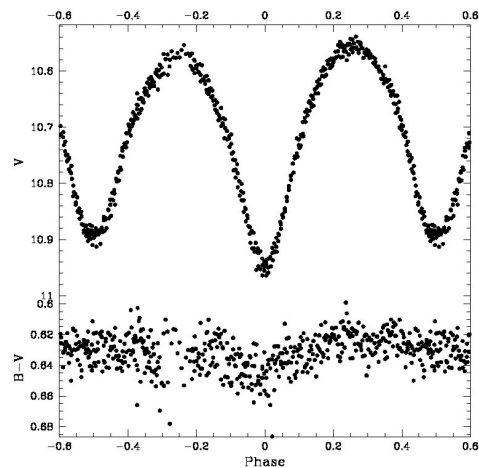


Figure 3. Folded light curve for differential aperture Johnson V-band magnitudes (top panel) and (B–V) color (bottom panel) versus orbital phase. Phase values are defined by Equation 1. Error bars are not shown for clarity. All (B–V) colors are calculated by subtracting linearly interpolated B magnitudes from measured V magnitudes.

PERANSO at 1σ deviation. For all subsequent fitting the orbital period of 0.33440 ± 0.00037 day will be assumed, and does not change any of the results of this study.

Effective temperature and spectral type are estimated from the (B–V) color index values measured at orbital quadrature ($\Phi = \pm 0.25$) with a value of $(B-V) = 0.63 \pm 0.03$. Interstellar extinction estimates following (Schlafly and Finkbeiner 2011) at the galactic coordinates for the object are $E(B-V) = 0.084$. The resulting intrinsic color becomes $(B-V)_0 = 0.54 \pm 0.03$. Effective temperatures and errors were estimated by Table 3 from Flower (1996) to be $T_{\text{eff}} = 6118 \pm 120\text{K}$. The corresponding stellar spectral type is a F8 (Fitzgerald 1970) with an estimated stellar mass $M_{\star} = 1.20^{+0.04}_{-0.03} M_{\odot}$ derived from Equation 4 of Harmanec (1988). It should be noted that these masses are for normal main sequence stars, and may be suspect. We include them in the analysis as an estimate on the stellar mass only. Furthermore, the 2MASS All Sky Survey (Skrutskie *et al.* 2006) reports a $(J-H) = 0.29 \pm 0.04$ for NSVS 3068865 which corresponds to a spectral type of F8 (Ducati *et al.* 2001) after correcting for interstellar extinction ($(J-H)_0 = 0.27 \pm 0.04$) following Schlafly and Finkbeiner (2011), and supports our prior claim despite the unknown orbital phase at which the 2MASS magnitudes were obtained. The semi-major axis (a) is determined by Kepler’s third law.

3.2. Light curve analysis

All observations taken during this study were analyzed using the Physics of Eclipsing Binaries (PHOEBE) software

package (v0.31a) (Prša and Zwitter 2005). The PHOEBE software package is a modeling package that provides a convenient, intuitive graphical user interface (GUI) to the Wilson-Devinney (WD) code (Wilson and Devinney 1971). Table 2 summarizes the authors’ analysis for NSVS 3068865.

All three Johnson-Cousins B, V, and R_c bands were fit simultaneously by the following procedure. Initial fits were performed assuming a common convective envelope in direct thermal contact resulting in a common surface temperature of $T_{\text{eff}} = 6118\text{K}$ determined by the procedure discussed in section 3.1. Orbital period was set to the value of 0.33440 ± 0.00037 day. Surface temperatures imply that the outer envelopes are convective so the gravity brightening coefficients β_1 and β_2 , defined by the flux dependency $F \propto g^{\beta}$, were initially set at the common value consistent with a convective envelope of 0.32 (Lucy 1967). The more recent studies of Alencar and Vaz (1997) and Alencar *et al.* (1999) predict values for $\beta \approx 0.4$. These values were also used but had no effect on the resulting best-fit model. We adopted the standard stellar bolometric albedo $A_1 = A_2 = 0.5$ as suggested by Ruciński 1969) with two possible reflections.

The fitting procedure was used to determine the best-fit stellar models and orbital parameters from the observed light curves shown in Figure 2. Initial fits were performed assuming a common convective envelope in thermal contact which assumes similar surface temperatures for both after normalization of the stellar luminosity, the light curve was crudely fit by altering the stellar shape by fitting the Kopal (Ω) parameter. The Kopal parameter describes the equipotential surface that the stars fill.

Table 2. Model parameters for NSVS 3068865 determined by the best-fit WD model.

Parameter	Symbol	Value		
		Stellar spots not allowed	Stellar Spots allowed	
Period	P_0 [days]	0.33440 ± 0.00037	0.33440 ± 0.00037	
Epoch	T_0 [HJD]	$2456487.66872 \pm 0.00026$	$2456487.66872 \pm 0.00026$	
Inclination	i [$^{\circ}$]	66.26 ± 0.29	66.00 ± 0.29	
Semimajor Axis ^a	a [R_{\odot}]	2.72 ± 0.20	2.72 ± 0.20	
Surface Temp.	$T_{\text{eff},1}$ [K]	$6118. \pm 120$	$6118. \pm 120$	
	$T_{\text{eff},2}$ [K]	$6066. \pm 120$	$6122. \pm 120$	
Surface Potential	$\Omega_{1,2}$ [—]	3.624 ± 0.043	3.570 ± 0.043	
Mass Ratio	q [—]	0.95 ± 0.02	0.92 ± 0.02	
Luminosity	$[L_1/(L_1 + L_2)]_B$	0.573 ± 0.005	0.571 ± 0.004	
	$[L_1/(L_1 + L_2)]_V$	0.559 ± 0.006	0.560 ± 0.005	
	$[L_1/(L_1 + L_2)]_{R_c}$	0.550 ± 0.008	0.552 ± 0.006	
Stellar Mass ^a	M_1 [M_{\odot}]	1.24 ± 0.24	1.26 ± 0.24	
	M_2 [M_{\odot}]	1.17 ± 0.24	1.15 ± 0.24	
Limb Darkening	$x_{\text{bol},1,2}$	0.644	0.644	
	$y_{\text{bol},1,2}$	0.225	0.225	
	$x_{B,1,2}$	0.823	0.823	
	$y_{B,1,2}$	0.197	0.197	
	$x_{V,1,2}$	0.736	0.736	
	$y_{V,1,2}$	0.262	0.263	
	$x_{R,1,2}$	0.644	0.644	
	$y_{R,1,2}$	0.271	0.271	
	Spot Colatitude	ϕ_1 [$^{\circ}$]	—	90
	Spot Longitude	λ_1 [$^{\circ}$]	—	0
Spot Radius	ρ_1 [$^{\circ}$]	—	45	
Temperature Factor	τ_1 [—]	—	0.95	

Notes: Values for the best fit stellar model not allowing for the presence of stellar spots (column 3) as well as best fit values for models allowing for the presence of stellar spots (column 4). Some parameters can be further specified by a the numerical value 1 for the primary stellar component, or 2 for the secondary stellar component. Fitting procedure is described in sections 3.2 and 3.3. Surface potentials for both stars for contact/overcontact binaries is defined to be of equal value for both stars. Errors for surface temperatures (T_{eff}) were estimated from color values in Figure 3. Please note that the parameters L_1 and L_2 refer to the luminosities of primary and secondary components, respectively. All remaining errors are 1σ errors. a) See section 3.1 for discussion.

For overcontact binaries, this has the effect of determining the shape of the stars, and has a strong effect on the the global morphology of the light curve.

After the fit no longer be improved, we started to consider the other parameters to fit the light curve. These additional parameters were also allowed to vary with the previous parameters and included the effective temperature of the secondary star $T_{\text{eff},2}$, the mass ratio $q = M_2 / M_1$ and the orbital inclination i . The mass ratio (q) was further refined after a standard q -search method was applied. In this method the mass ratio is fixed and all other parameters are allowed to converge to a best-fit model. The χ^2 values (sum of the squares of the residuals) are recorded for each fixed value of the mass ratio. The reported mass ratio is the minimum in the resulting curve. Minor improvement of the of the best-fit model could be achieved by decoupling stellar luminosities from T_{eff} . We interpreted this as the possibility that the stars are in poor thermal contact and therefore could have differing surface temperatures. All further model fits were performed assuming the primary and secondary components are in poor thermal contact.

All model fits were performed with a limb darkening correction. PHOEBE allows for differing functional forms to be specified by the user. Late-type stars ($T_{\text{eff}} < 9000\text{K}$) are best described by the logarithmic law that was first suggested by Klingsmith and Sobieski (1970), and later supported by the more recent studies of Diaz-Cordoves and Gimenez (1992) and van Hamme (1993). The values for the linear (x_λ) and non-linear (y_λ) coefficients were determined at each fitting iteration by the van Hamme (1993) interpolation tables.

Figures 4 through 6 show the folded Johnson B, Johnson V, and Cousins R_c band light curves along with the synthetic light curve calculated by the best-fit model, respectively. The best-fit models were determined by the aforementioned fitting procedure. Note how the synthetic light curve consistently over-predicts the observed light curve for phases in the interval $(-0.3, 0.1)$, and under-predicts for phases in the interval $(0.3, 0.5)$. The parameters along with 1σ error bars describing this best-fit model are given in column 3 of Table 2.

The filling factor is defined by the inner and outer critical equipotential surfaces that pass through the L_1 and L_2 Lagrangian points of the system, and is given by the following equation:

$$\mathcal{F} = \frac{\Omega(L_1) - \Omega}{\Omega(L_1) - \Omega(L_2)} \quad (3)$$

where Ω is the equipotential surface describing the stellar surface, and $\Omega(L_1)$ and $\Omega(L_2)$ are the equipotential surfaces that pass through the Lagrangian points L_1 and L_2 , respectively. For our system the these equipotential surfaces are $\Omega(L_1) = 3.669$ and $\Omega(L_2) = 3.149$. The best-fit model is consistent with an overcontact binary described by a filling factor $\mathcal{F} = 0.09 \pm 0.04$.

3.3. Spot model

It is apparent from Figures 4 through 6 that the previous model is unable to reproduce accurately the observed light curve. To improve the fit, a single spot was necessary. Unfortunately, all we have at our disposal are the observed light curves, and

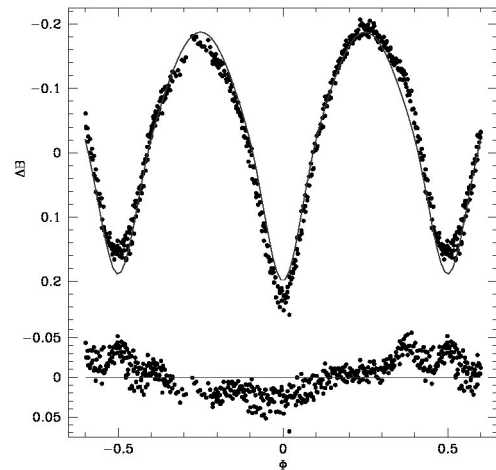


Figure 4. Best-fit WD model fit without spots (solid curve) to the folded light curve for differential Johnson B band magnitudes (top panel). The best-fit orbital parameters used to determine the light curve model are given in Table 2. The bottom panel shows residuals from the best-fit model (solid curve). Error bars are omitted from the points for clarity.

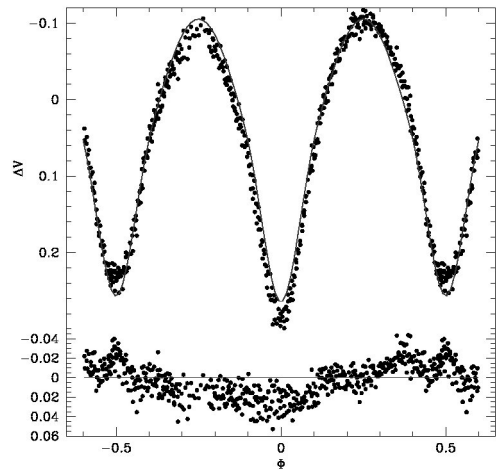


Figure 5. Best-fit WD model fit without spots (solid curve) to the folded light curve for differential Johnson V band magnitudes (top panel). The best-fit orbital parameters used to determine the light curve model are given in Table 2. The bottom panel shows residuals from the best-fit model (solid curve). Error bars are omitted from the points for clarity.

differing spot models may be degenerate to the observed light curve.

The best-fit model with a single cool spot on the primary star is given in Table 2. Spot parameters given by the WD model are the longitude θ , colatitude ϕ , radius ρ , and temperature factor ($\tau = T_{\text{spot}} / T_{\text{eff}}$). The spot longitude is measured counterclockwise (CCW) from the L_1 Lagrangian point. Spot colatitude is measured from stellar rotation axis with the equator represented by $\phi = 90^\circ$. Light curves were found to be minimally dependent on the spot's colatitude and therefore difficult to converge when allowed to vary. All spot models restricted spots to be located on the equator ($\phi = 90^\circ$).

Initial models started from the model without spots determined in section 3.2. We were unsuccessful with simultaneous convergence of the parameters. The spot longitude eluded successful convergence, and forced a manual procedure. But both the spot radius and the spot temperature factor did

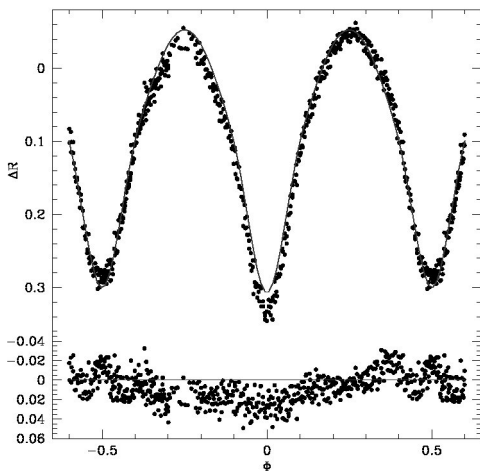


Figure 6. Best-fit WD model fit without spots (solid curve) to the folded light curve for differential R_C band magnitudes (top panel). The best-fit orbital parameters used to determine the light curve model are given in Table 2. The bottom panel shows residuals from the best-fit model (solid curve). Error bars are omitted from the points for clarity.

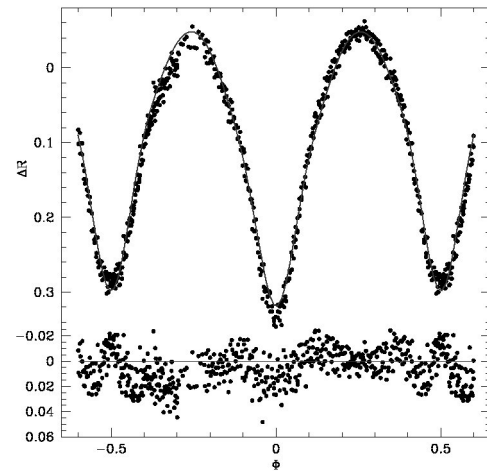


Figure 9. Best-fit WD model fit with a single spot (solid curve) to the folded light curve for differential R_C band magnitudes (top panel). The best-fit orbital parameters used to determine the light curve model are given in Table 2. The bottom panel shows residuals from the best-fit model (solid curve). Error bars are omitted from the points for clarity.

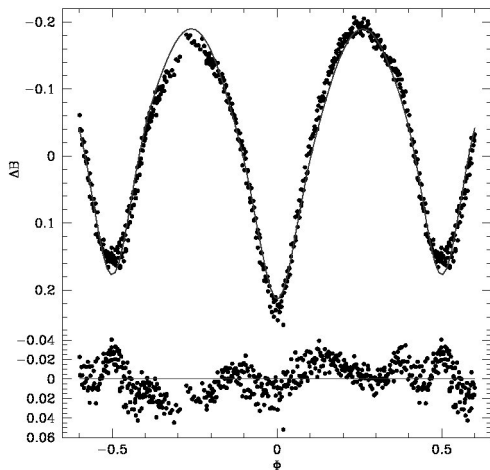


Figure 7. Best-fit WD model fit with a single spot (solid curve) to the folded light curve for differential Johnson B band magnitudes (top panel). The best-fit orbital parameters used to determine the light curve model are given in Table 2. The bottom panel shows residuals from the best-fit model (solid curve). Error bars are omitted from the points for clarity.

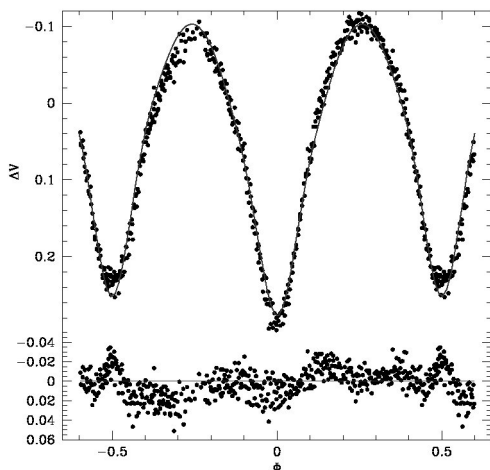


Figure 8. Best-fit WD model fit with a single spot (solid curve) to the folded light curve for differential Johnson V band magnitudes (top panel). The best-fit orbital parameters used to determine the light curve model are given in Table 2. The bottom panel shows residuals from the best-fit model (solid curve). Error bars are omitted from the points for clarity.

converge individually, but not conjointly. The best-fit spot model was determined by alternating between convergence of the spot radius and the spot temperature factor. Once a satisfactory convergence was determined, the spot parameters were then held fixed and the stellar parameters were then allowed to converge to the final model. Figures 7 through 9 show the final best-fit stellar model. Graphical representations for the best-fit spot WD model are shown in Figure 12.

Our best-fit spot model does fit the observed data well, but as noted above may be degenerate to alternate possible explanations for the observed deviations shown in Figures 4 through 6. The spot determined by the spot fitting procedure described above covers the majority of the hemisphere facing the stellar juncture (L_1) with a weak temperature factor $\tau \approx 1$.

4. Discussion and conclusions

Figure 10 shows a comparison of the NSVS light curve with the light curve measured during this study. It is immediately apparent that both the NSVS light curve and the light curve measured during this study show similar heights for max I ($\phi = 0.25$) and max II ($\phi = -0.25$). Differing heights between max I and max II is known as the O'Connell effect (O'Connell 1951) and is not uncommon in overcontact binaries. Temporal variance of this effect has also been observed, but evidence for the O'Connell effect in NSVS 3068865 is minimal.

Recent studies have shown that degeneracies exist between the orbital inclination (i), mass ratio (q), and filling factor ($\mathcal{F}(\Omega)$) for partially eclipsing overcontact binaries (Terrell and Wilson 2005; Hambálek and Pribulla 2013). To investigate these degeneracies, we generated ten groups of B, V, R_C synthetic light curves from the observed light curve by the following procedure. Prior studies have shown that partially eclipsing overcontact binaries are accurately (rms residuals ~ 0.0002) represented by a Fourier series of 10th order (Rucinski 1993; Hambálek and Pribulla 2013). A mean light curve was first generated by fitting the observed light curve with a Fourier

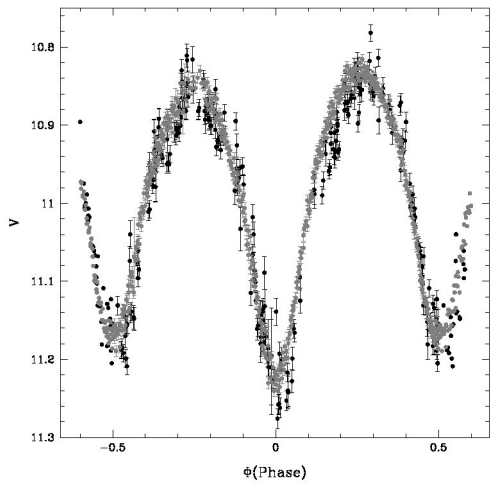


Figure 10. Folded light curve for Johnson V magnitudes. Grey points are measured magnitudes from the Ball State University 0.4m telescope. Measured values from the NSV Survey (Woźniak *et al.* 2004) are shown by the black points. Any systematic offsets resulting from the calibration of the unfiltered CCD magnitudes of the NSV survey (see text) are removed for comparison of light curves. All error bars are 1σ error bars. Repeated points do not show error bars.

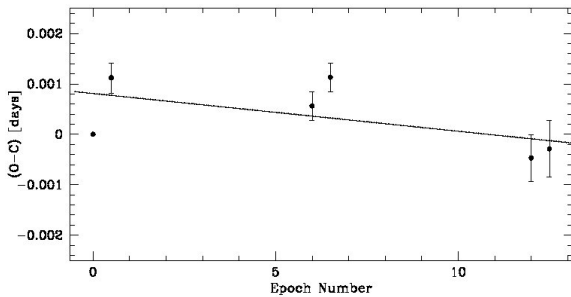


Figure 11. Observed minus calculated residual times of minimum (O-C) versus orbital epoch number. All point values are given in Table 1. Secondary times of minimum are plotted at half integer values, and all error bars are 1σ error bars. Solid curve shows the best-fit linear line determined by a linear regression fit to the (O-C) residual values.

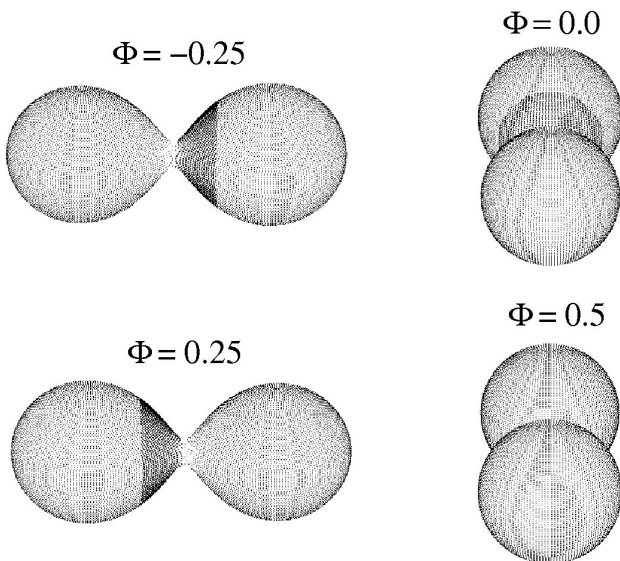


Figure 12. Graphical representation for the best-fit single spot WD model. The best-fit orbital parameters used to determine the light curve model are given in Table 2. Corresponding orbital phase is given in each panel.

series of 10^{th} order. The synthetic light curve is then generated by adding a Gaussian deviate of standard deviation equal to the photometric error of the observed data point to the mean value generated by the Fourier representation at a similar phase determined by Equation 2. Solutions were obtained from three randomly selected starting points in the $[i, q, \Omega]$ parameter space for each of the ten synthetic light curve groups. All fits were run without any user input or guidance. We found our solution for the light curves to be remarkably robust. The errors reported for the best-fit parameters in Table 2 reflect the standard deviation of the range of values resulting for the synthetic light curve solutions. It is possible that degeneracies still exist in the $[i, q, \Omega]$ parameter space, but will require spectroscopic followup of NSVS 3068865 to break these degeneracies.

Given the best-fit model parameters in Table 2, we can estimate the distance to NSVS 3068865. (Rucinski and Duerbeck 1997) determined that the absolute visual magnitude is given by

$$M_V = -4.44 \log_{10}(P) + 3.02(B-V)_0 + 0.12 \quad (4)$$

to within an accuracy of ± 0.1 . The distance modulus of the system $(m - M) = 6.44$. After accounting for the extinction ($A_V = 0.26$) determined from color excess given in section 3.1, we determined the distance to the system is 194 ± 10 pc. Distance errors do not account for possible errors in the extinction maps of Schlafly and Finkbeiner (2011).

This study has confirmed that NSVS 3068865 is a W UMa contact binary in or near thermal contact. Our measured light curve does not show conclusive evidence of the O’Connell effect, and was fairly well described by the stellar orbital parameters alone. The star NSVS 3068865 appears to be consistent with a slightly larger primary component eclipsed during the primary minimum. A spot model with a single spot did improve the best-fit model. However, deviations from the light curve determined by the orbital parameters alone could not account for all the observed variation. We favored a single spot model with a weak temperature factor covering the hemisphere centered on the stellar juncture. This system shows similarities to the prototype W Ursae Majoris. Both systems are members of the W-subclass with similar orbital periods (Linnell 1991). While W UMa has shown to have an unpredictable O’Connell effect (Linnell 1991), NSVS 3068865, with a comparison to the previously measured NSVS data (Woźniak 2004), appears to have stable maxima of comparable brightness (see Figure 10). Further spectroscopic follow up will be necessary to place further constraints and to validate the stellar masses and orbital parameters to further improve our knowledge of the system.

5. Acknowledgements

We wish to thank both the referee and Edward Devinney for their detailed and constructive comments.

References

Alencar, S. H. P., and Vaz, L. P. R. 1997, *Astron. Astrophys.*, **326**, 257.

- Alencar, S. H. P., Vaz, L. P. R., and Nordlund, Å. 1999, *Astron. Astrophys.*, **346**, 556.
- Berry, R., and Burnell, J. 2005, *Handbook of Astronomical Image Processing*, Willmann-Bell, Richmond.
- CBA Belgium Observatory. 2011, PERANSO (v2.51) software, Flanders, Belgium (<http://www.cbabelgium.com/>).
- Diaz-Cordoves, J., and Gimenez, A. 1992, *Astron. Astrophys.*, **259**, 227.
- Ducati, J. R., Bevilacqua, C. M., Rembold, S. B., and Ribeiro, D. 2001, *Astrophys. J.*, **558**, 309.
- Fitzgerald, M. P. 1970, *Astron. Astrophys.*, **4**, 234.
- Flower, P. J. 1996, *Astrophys. J.*, **469**, 355.
- Gettel, S. J., Geske, M. T., and McKay, T. A. 2006, *Astron. J.*, **131**, 621.
- Hambálek, Ľ., and Pribulla, T. 2013, *Contrib. Astron. Obs. Skalnaté Pleso*, **43**, 27.
- Harmanec, P. 1988, *Bull. Astron. Inst. Czechoslovakia*, **39**, 329.
- Hoffman, D. I., Harrison, T. E., and McNamara, B. J. 2009, *Astron. J.*, **138**, 466.
- Høg, E., *et al.* 2000, *Astron. Astrophys.*, **355**, L27.
- Klinglesmith, D. A., and Sobieski, S. 1970, *Astron. J.*, **75**, 175.
- Kwee, K. K., and van Woerden, H. 1956, *Bull. Astron. Inst. Netherlands*, **12**, 327.
- Linnell, A. P. 1991, *Astrophys. J.*, **374**, 307.
- Lucy, L. B. 1967, *Z. Astrophys.*, **65**, 89.
- O'Connell, D. J. K. 1951, *Publ. Riverview Coll. Obs.*, **2**, 85.
- Prša, A., and Zwitter, T. 2005, *Astrophys. J.*, **628**, 426.
- Ruciński, S. M. 1969, *Acta Astron.*, **19**, 245.
- Rucinski, S. M. 1993, *Publ. Astron. Soc. Pacific*, **105**, 1433.
- Rucinski, S. M., and Duerbeck, H. W. 1997, *Publ. Astron. Soc. Pacific*, **109**, 1340.
- Schlafly, E. F., and Finkbeiner, D. P. 2011, *Astrophys. J.*, 737, 103.
- Schwarzenberg-Czerny, A. 1996, *Astrophys. J., Lett. Ed.*, **460**, L107.
- Skrutskie, M. F., *et al.* 2006, *Astron. J.*, **131**, 1163.
- Terrell, D., and Wilson, R. E. 2005, *Astrophys. Space Sci.*, **296**, 221.
- van Hamme, W. 1993, *Astron. J.*, **106**, 2096.
- Wilson, R. E., and Devinney, E. J. 1971, *Astrophys. J.*, **166**, 605.
- Woźniak, P. R., *et al.* 2004, *Astron. J.*, **127**, 2436.